

Analysis of the fluorescence temporal point-spread function in a turbid medium and its application to optical imaging

Sung-Ho Han
Salman Farshchi-Heydari
David J. Hall

University of California at San Diego
Moore's Cancer Center and Department of Radiology
3855 Health Sciences Drive, 0819
La Jolla, California 92093-0819
E-mail: sunghohan@ucsd.edu

Abstract. A time-domain optical method to evaluate the concentration (n), lifetime (τ), and depth (d) of a fluorescent inclusion is described by the complete analysis of the fluorescence temporal point-spread function (TPSF). The behavior of parameters in the fluorescence TPSF is explored, and we demonstrate the method with experimental data from a localized fluorescent inclusion in scattering media to recover images of n , τ , and d . The method has potential application for *in vivo* fluorescence imaging. © 2008 Society of Photo-Optical Instrumentation Engineers. [DOI: 10.1117/1.3042271]

Keywords: time domain; fluorescence; scattering media.

Paper 08224R received Jul. 10, 2008; revised manuscript received Oct. 28, 2008; accepted for publication Oct. 29, 2008; published online Dec. 18, 2008.

1 Introduction

Cancer is a major public health problem worldwide. Currently, one in four deaths in the United States is caused by cancer.¹ Breast cancer has been one of the dominant causes for the deaths of women in the United States.¹ Since breast cancer is spread easily by metastasis, its early detection is crucial. Systematic use of x-ray mammography has been extremely beneficial in detecting breast cancer and is the gold standard. However, the potential risk related with repetitive exposure to this ionizing radiation technique² has led to the development of complementary diagnostic methods using nonionizing techniques such as near-infrared (NIR) optical imaging.^{3,4}

Optical fluorescence molecular imaging has the potential to provide clinical information in biomedical applications such as tissue oxygenation, glucose levels, and small molecule protein-protein interactions⁵ as well as the early detection of cancer. There are two main approaches to optical fluorescence molecular imaging in a tissue-like turbid medium: continuous-wave (cw) intensity measurement and time-domain (TD) measurement (or its frequency domain equivalent), where the fluorescence temporal response (order of nanoseconds) to a short pulse (order of picoseconds) of excitation light is recorded and known as a fluorescence temporal point-spread function (TPSF). The cw technique is most widely used due to its simple and inexpensive implementation. However, unlike the cw technique that typically provides 2-D images of fluorescent cw intensity, the TD technique has the opportunity to further provide the concentration (n), lifetime (τ), and depth (d) of a fluorescent inclusion. cw tomographic methods have been adopted to try and solve the problem of decoupling fluorescence intensity into n and d , where multiple source-detector pair cw measurements are acquired at many

angles with complicated and intensive inversion processes.⁶ Alternatively, only one source-detector pair measurement is needed to recover n and d with a TD technique, as previously published.⁷ More recently,⁸ we described a simple method for recovering τ and d of a fluorescent inclusion from direct evaluations of the temporal position of the fluorescence temporal point-spread function (TPSF) maximum (t_{\max}) and the exponential time decay of a given fluorescence TPSF, so-called effective lifetime (τ_{eff}). Here, we simultaneously evaluate all three parameters, i.e., n , τ , and d of a fluorescent inclusion, by fitting the complete fluorescence TPSF with an analytical diffusion model of photon propagation.

2 Theory

2.1 Photon Migration in a Turbid Medium

Ultimately, the best way to provide a thorough description of a photon migration in a turbid medium is TD diffuse optical tomography, which decouples the underlying scattering and absorption of photons. NIR photon migration in a turbid medium is governed by the diffusion equation for the diffuse photon fluence rate $\varphi(\mathbf{r}, t)$,

$$-\nabla \cdot [D(\mathbf{r}) \nabla \varphi(\mathbf{r}, t)] + \frac{1}{v} \frac{\partial \varphi(\mathbf{r}, t)}{\partial t} + \mu_a(\mathbf{r}) \varphi(\mathbf{r}, t) = S(\mathbf{r}_s, t), \quad (1)$$

where v is the speed of light in the medium, $\mu_a(\mathbf{r})$ is the optical absorption coefficient, $\mu_s(\mathbf{r})$ is the optical scattering coefficient, g is the mean cosine of the scattering angle, $S(\mathbf{r}_s, t)$ is the photon source at a source location (\mathbf{r}_s), $D(\mathbf{r}) = \{3[\mu_a(\mathbf{r}) + \mu'_s(\mathbf{r})]\}^{-1}$ is the diffusion coefficient, and $\mu'_s(\mathbf{r}) = (1 - g)\mu_s(\mathbf{r})$ is the reduced scattering coefficient. $D(\mathbf{r})$ is usually approximated to be $[3\mu'_s(\mathbf{r})]^{-1}$, since scattering is dominant over absorption in a turbid medium. For a short

Address all correspondence to Sung-Ho Han, Radiology, University of California, San Diego, 3855 Health Sciences Drive #0819-La Jolla, CA 92093-0819; Tel: 858-822-2594; Fax: 858-822-0950; E-mail: sunghohan@ucsd.edu

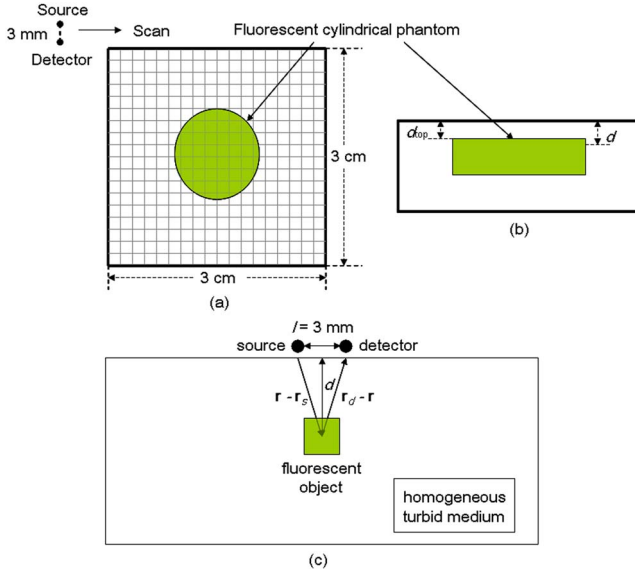


Fig. 1 (a) Reflection geometry is composed of a single source-detector pair (3-mm separation), which is raster scanned every 2 mm across the phantom surface ($3 \times 3 \text{ cm}^2$ area) encompassing the submerged fluorescent inclusion. (b) Side view of (a). (c) Schematic diagram of the experimental setup for the propagator description of photon migration.

pulse from an isotropic point source, if we assume that $\mu_a(\mathbf{r})$ and $\mu'_s(\mathbf{r})$ are position independent, i.e., $\mu_a(\mathbf{r}) = \mu_a$ and $\mu'_s(\mathbf{r}) = \mu'_s$, then the solution to Eq. (1) becomes Green's function.^{9,10}

$$G(\mathbf{r}, t) = \frac{1}{(4\pi Dvt)^{3/2}} \exp\left(-\frac{r^2}{4Dvt} - \mu_a vt\right), \quad (2)$$

which describes the light propagation in a turbid medium.

2.2 Light Propagation Model

A schematic diagram of the experimental setup of the eXplore OptixTM-MX2 system (ART Advanced Research Technologies, Inc., Montreal, Canada) is shown in Fig. 1(c). As shown in Fig. 1(c), the whole light propagation procedure from source to detector can be divided into four steps: [f_1] Green's function representing a photon migration from source (\mathbf{r}_s) to a fluorescent inclusion (\mathbf{r}), [f_2] lifetime decay (τ) of a fluorescent inclusion, [f_3] another Green's function showing a migration from a fluorescent inclusion (\mathbf{r}) to detector (\mathbf{r}_d), and [f_{IRF}] impulse response function (IRF) of approximated Gaussian wave form. In general, μ_a and μ'_s are functions of wavelength, thus the steps [f_1] and [f_3] should be described by different propagators. However, since the excitation and emission wavelength are close to each other where tissue optical properties vary slowly, these Green's functions can be described by the same propagator. A summary of the previous procedure can be written as the forms of the following analytical functions,

$$f_1 = G(|\mathbf{r} - \mathbf{r}_s|, t), \quad f_2 = \left[\frac{n(r)\exp(-t/\tau)}{\tau} \right], \quad (3)$$

$$f_3 = G(|\mathbf{r}_d - \mathbf{r}|, t), \quad f_4 = \exp\left[-\frac{(t - t_{\text{IRF}})^2}{\sigma_{\text{IRF}}^2}\right],$$

where τ is a lifetime of a fluorescent inclusion and t_{IRF} represents the central temporal position of the Gaussian IRF with a width of σ_{IRF} . Under this formulation, the use of the standard first-order Born approximation^{11,12} gives us a resulting reflective fluorescence fluence rate at a detector position from a fluorophore distributed in a volume V ,

$$\varphi(\mathbf{r}_s, \mathbf{r}_d, t) = C \int_V d\mathbf{r} f_1 * f_2 * f_3 * f_{\text{IRF}}, \quad (4)$$

where C is a constant including source/detector efficiencies and a filter loss. Here $n(\mathbf{r})$ represents the product of the concentration and its quantum efficiency (which is known *a priori*), and $*$ denotes the convolution.

To generate a fluorescent distribution in the region of interest, the integral in Eq. (4) is to be discretized [\mathbf{r} , $n(\mathbf{r})$, $\tau(\mathbf{r})$, $\mu_a(\mathbf{r})$, $\mu'_s(\mathbf{r}) \rightarrow \mathbf{r}_j$, $n_j(\mathbf{r})$, $\tau_j(\mathbf{r})$, $[\mu_a(\mathbf{r})]_j$, $[\mu'_s(\mathbf{r})]_j$]. For a series of measurements that have been made at source [$(\mathbf{r}_s)_i$] and detector [$(\mathbf{r}_d)_i$] positions, Eq. (4) turns to the following matrix equation,

$$\varphi_i[(\mathbf{r}_s)_i, (\mathbf{r}_d)_i, t] = \sum_{j=1}^N G[|\mathbf{r}_j - (\mathbf{r}_s)_i|, t] * \left[\frac{n_j(\mathbf{r}_j)\exp(-t/\tau)}{\tau_j} \right] * G[|(\mathbf{r}_d)_i - \mathbf{r}_j|, t] * \exp\left[-\frac{(t - t_{\text{IRF}})^2}{\sigma_{\text{IRF}}^2}\right]. \quad (5)$$

3 Materials and Methods

3.1 The eXplore OptixTM-MX2 System

The eXplore OptixTM-MX2 system is the only commercially available multiwavelength (470, 635, 670, and 760 nm) TD optical molecular imaging system for small animals.¹³ The laser pulse width was approximately 70 ps and the temporal resolution of the detection system was approximately 250 ps. Schematic scanning geometry is depicted in Figs. 1(a) and 1(b). Scanning resolution was 2 mm per step over the region of interest (ROI) with a scan time of 1 s per step. The ROI was a square of area $3 \times 3 \text{ cm}^2$ within which a small cylindrical Cy5 or Cy7 inclusion was submerged in the optical scattering Intralipid medium. The system uses a single source-detector configuration to scan the small animal in reflection mode, and measures the fluorescence TPSF for each scanned pixel. The fluorescence TPSFs were used to quantify n , τ , and d of the fluorescent inclusion.

3.2 Phantom Manufacture

To expedite repeated and robust experiments, we manufactured solid optically scattering fluorescent pellets with either Cy5 or Cy7 at $10 \mu\text{M}$, similar to a method that is found in the literature.¹⁴ The diameter and the height of these cylindrical pellets were 15 and 8 mm, respectively.

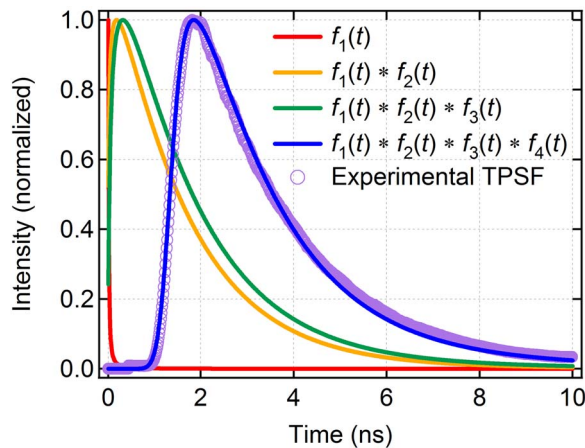


Fig. 2 Temporal evolution of the maximum intensity normalized fluorescence TPSF at each step during photon migration from source to detector.

4 Results and Discussion

4.1 Temporal Evolution of the Light Propagation

In the forward problem we use Eq. (4) to model the light propagation and resulting fluorescence TPSF given *a priori* optical properties of a turbid medium and the fluorophore inclusion properties. Figure 2 shows the evolution of the fluorescence TPSF at each propagation step with normalized maximum intensity to highlight the increasing temporal convolution form. To validate the forward model, we used the optical properties from the phantom experiment with a Cy5 fluorophore inclusion (i.e., $\mu_a = 3.0 \times 10^{-4} \text{ mm}^{-1}$, $\mu'_s = 1.3 \text{ mm}^{-1}$, $\tau = 1.5 \text{ ns}$, and $d = 1 \text{ mm}$). Rather than attempting to calibrate the experiment intensity units to model intensity units, we simply display the normalized maximum intensity experimental data in Fig. 2 and demonstrate that the forward model can predict the correct shape of the experimental fluorescence TPSF. Moreover, since the model assumes a point fluorophore and experimentally we have a finite fluorescent inclusion, it is not strictly possible to model the absolute fluorophore concentration, although we can still compare fluorophore concentration in arbitrary units within this point-model approximation. From Fig. 2 it can also be seen that the time decay of the fluorescence TPSF is largely dominated by the lifetime decay of the fluorescent inclusion. However, the so-called effective lifetime τ_{eff} indicating the time decay of a fluorescence TPSF is not the same as the actual lifetime τ of a fluorescent inclusion due to the convolution of its lifetime decay with two Green's functions and the IRF. For more detailed analysis, the increase in the decay of the fluorescence TPSF is evaluated by fitting it with a monoexponential function from 80% peak intensity to 20% peak intensity as the photons propagate from source to detector. The first Green's function $[f_1(t)]$, i.e., the propagation of light from source (\mathbf{r}_s) to a fluorescent inclusion (\mathbf{r}) in a turbid medium, shows a rapid decay of only 33 ps, which does not contribute significantly to the effective lifetime of the resultant fluorescence TPSF, which is 1.98 ns. After photons excite the fluorescent inclusion to cause fluorescence emission, the decay of the consequent function $[f_1(t) * f_2(t)]$ is 1.64 ns, which is a sig-

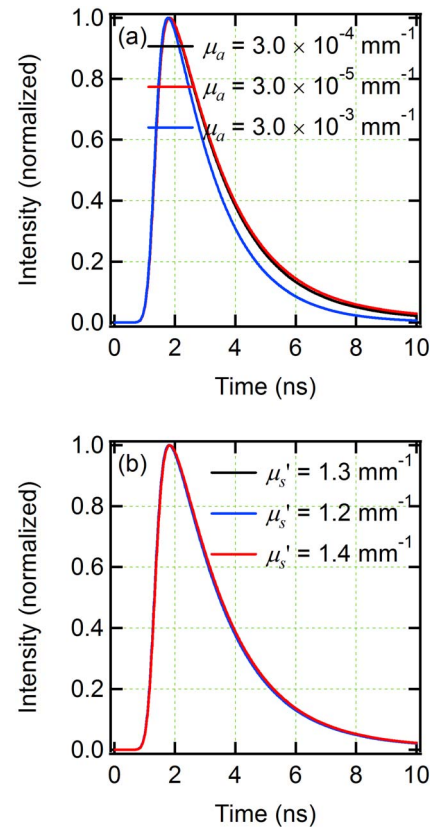


Fig. 3 Maximum intensity normalized fluorescence TPSFs for varying background optical properties for (a) $\mu_a = 3.0 \times 10^{-5} - 3.0 \times 10^{-3} \text{ mm}^{-1}$ and (b) $\mu'_s = 1.2$ to 1.4 mm^{-1} .

nificant component of the effective lifetime. When convoluted with another Green's function $[f_3(t)]$, there is a slight increase in the decay of the consequent function $[f_1(t) * f_2(t) * f_3(t)]$ to 1.78 ns. Finally, convolution with the system IRF $[f_{\text{IRF}}]$ adds further increase, resulting in the fluorescence TPSF $[f_1(t) * f_2(t) * f_3(t) * f_{\text{IRF}}(t)]$, whose decay is 1.98 ns and is the effective lifetime.

4.2 Effect of Background Optical Properties on the Fluorescence Temporal Point-Spread Function

We assumed the background optical properties were known accurately *a priori*. However, *in vivo* we have to estimate the optical properties of the mouse where inaccuracy can introduce error in recovering n , τ , and d of the fluorophore. To mimic this condition, we used the forward model to generate fluorescence TPSFs for a variety of background optical properties (5% change in μ_a or μ'_s from initial values). We then fitted these fluorescence TPSFs with the model fixing the background optical properties to the initial values and investigated the impact on the recovered fitted values of n , τ , and d . We found that there was negligible error in τ and d (0.5%). Interestingly, Fig. 3 shows the fluorescence TPSFs normalized to maximum intensity, where it is observed that the temporal shape of the fluorescence TPSF for the different values of μ_a [Fig. 3(a)] and μ'_s [Fig. 3(b)] is similar. Since previous work⁸ has shown that τ and d are strongly correlated with the temporal shape of the fluorescence TPSF, i.e., τ_{eff} and t_{max} , it is

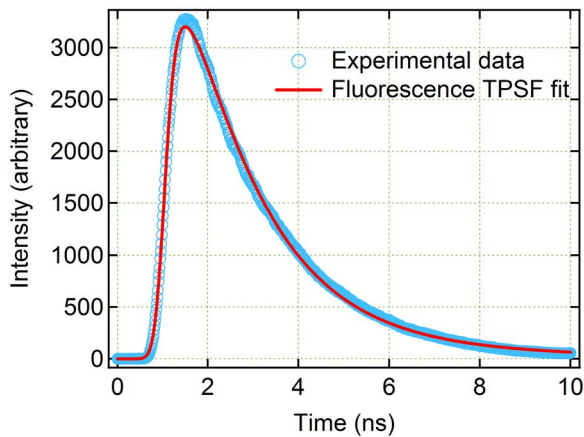


Fig. 4 Example fit result from Cy5 inclusion using the algorithm described in Eq. (5) with *a priori* values of $\mu_a=3.0 \times 10^{-4} \text{ mm}^{-1}$, $\mu'_s=1.31 \text{ mm}^{-1}$, $t_{\text{IRF}}=1.00 \text{ ns}$, and $\sigma_{\text{IRF}}=0.25 \text{ ns}$ at $\lambda=635 \text{ nm}$. Recovered fit values are evaluated as $n=6.5 \times 10^4 \text{ mm}^{-3}$, $\tau=1.52 \text{ ns}$, and $d=1.3 \text{ mm}$.

expected that similar τ and d values were recovered. However, varying the background optical properties also influences the absolute area of the fluorescence TPSF, which was found to induce a 10% error in n that essentially scales the intensity signal without changing the temporal shape. Nevertheless, recovery of fluorophore concentration within 10% would still be a useful result, given that the background optical properties can be estimated *a priori* within 5%.

4.3 Phantom Analysis

In this section we analyze experimental phantom data from Cy5 and Cy7 fluorescent inclusions submerged in a turbid medium. The background optical properties of the phantom were as follows: $\mu_a=3.0 \times 10^{-4} \text{ mm}^{-1}$, $\mu'_s=1.3 \text{ mm}^{-1}$ at $\lambda=635 \text{ nm}$ (for Cy5), and $\mu_a=2.0 \times 10^{-3} \text{ mm}^{-1}$, and $\mu'_s=1.0 \text{ mm}^{-1}$ at $\lambda=760 \text{ nm}$ (for Cy7).¹⁵ The eXplore-Optix-MX2 scanned the phantom and acquired fluorescence TPSFs as described before. Model fitting involved first averaging the fluorescence TPSFs from a region of interest covering the fluorescent pellet to extract an average value of n , τ , and d with *a priori* background optical properties. Using the average values as an initial guess, we then fitted the model [Eq. (5)] on a pixel-by-pixel basis. The difference between the measured and calculated fluorescence TPSF in each pixel was minimized using a least-squares nonlinear optimization routine, i.e., the Levenberg-Marquardt algorithm.^{16,17} For example, Fig. 4 shows a final fit result for a given pixel from the Cy5 fluorescent inclusion after 88 iterations from initial average parameters with *a priori* knowledge of the background optical properties ($\mu_a=3.0 \times 10^{-4} \text{ mm}^{-1}$ and $\mu'_s=1.3 \text{ mm}^{-1}$), as well as $t_{\text{IRF}}=1.00 \text{ ns}$, and $\sigma_{\text{IRF}}=0.25 \text{ ns}$ at $\lambda=635 \text{ nm}$. Recovered fitted values of $n=6.5 \times 10^4 \text{ mm}^{-3}$, $\tau=1.5 \text{ ns}$, and $d=1.3 \text{ mm}$ were obtained.

Displaying the recovered fitted values of n , τ , and d for each scanned pixel generated corresponding 2-D images of these parameters. Since the model assumes a point fluoro-

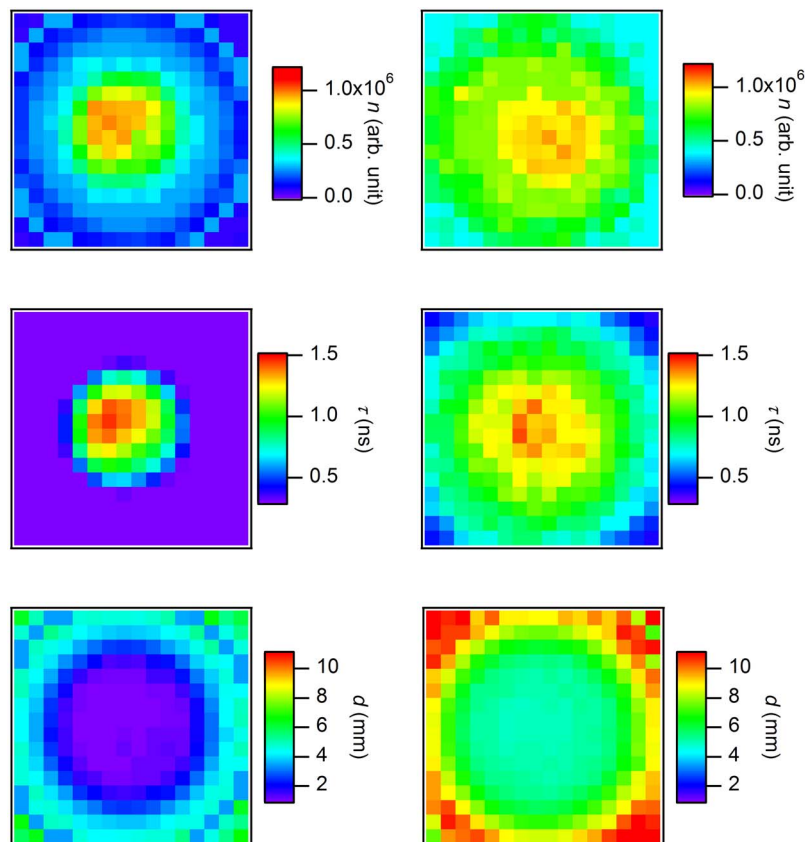


Fig. 5 Images of n (top row), τ (middle row), and d (bottom row) for shallowly (left) and deeply (right) embedded Cy5 inclusion.

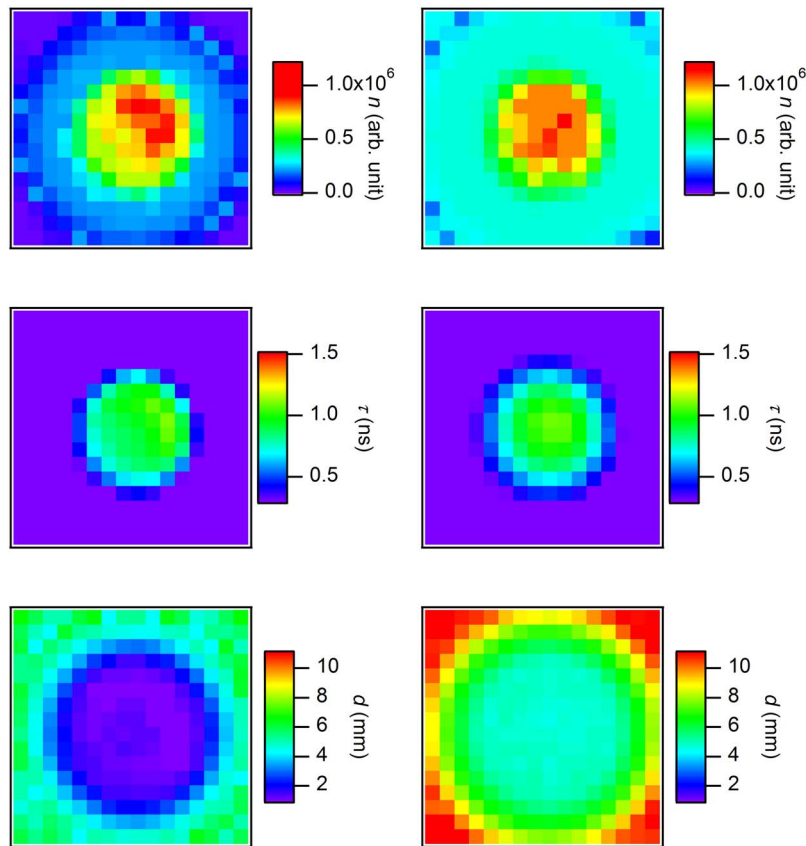


Fig. 6 Images of n (top row), τ (middle row), and d (bottom row) for shallowly (left) and deeply (right) embedded Cy7 inclusion.

phore at depth d directly below the surface, we recover appropriate values for the inclusion as we scan across it. However, as we scan away from the inclusion, the model breaks down and we no longer recover appropriate values. In essence, the model corrects for optical propagation in the z axis but not in the x - y scanning plane where optical scattering increases the apparent size of the inclusion. Figure 5 shows images of n (top row), and d (bottom row) of the Cy5 fluorescent inclusion submerged at 1 mm (left) and 5 mm (right), respectively. Figure 6 shows the corresponding images for the Cy 7 fluorescent inclusion. In Fig. 5 (top), it is seen in the vicinity of the inclusion that similar values of n ($\sim 1.0 \times 10^6$) are recovered at 1- and 5-mm submersion as expected, since the fluorophore concentration remained constant, even though the cw intensity diminished with increasing depth. In Fig. 5 (middle), it is seen in the vicinity of the inclusion that similar values of τ (~ 1.5 ns) are recovered at 1- and 5-mm submersion as expected, since the fluorophore lifetime remained constant even though the effective lifetime increased with increasing depth. In Fig. 5 (bottom), it is seen in the vicinity of the inclusion that different values of d (~ 1.3 and 5.4 mm) are recovered at 1- and 5-mm submersion as expected, since the fluorophore depth increased. Note the submersion depth is defined as the perpendicular distance to the top surface of the fluorescent inclusion. Given that we have a point model and a finite inclusion, it is expected to slightly overestimate d , as discussed elsewhere.⁸ Similar results were found for the Cy 7 fluorescent inclusion as seen in Fig. 6, where fitted values of

n ($\sim 1.2 \times 10^6$), τ (~ 1 ns), and d (~ 1.3 and 5.2 mm) were recovered.

5 Conclusion

A time-domain optical method to evaluate the concentration, lifetime, and depth of a fluorescent inclusion is described by the complete analysis of the fluorescence temporal point-spread function (TPSF). The sensitivity of these parameters to *a priori* estimates of background optical properties is explored. We demonstrate the approach by fitting the model to experimental data from a localized fluorescent inclusion in scattering media. 2-D images of n , τ , and d parameters are created from either Cy5 and Cy7 fluorescent inclusions submerged at depths of 1 or 5 mm. The model is able to recover the correct submersion depths, which also yield similar fluorophore concentrations and similar correct lifetimes as expected. Optical scattering still blurs the images in the x - y plane, and we plan to address this in future work. The method has potential applicability for *in vivo* fluorescence imaging where the point model is found to be adequate, i.e., localized fluorescent tumors.

Acknowledgments

The authors gratefully acknowledge the UCSD Department of Radiology and the NIH (grant No. S10 RR22599-01A1) for funding this work.

References

1. A. Jemal, R. Siegel, E. Ward, T. Murray, J. Xu, and M. J. Thun, "Cancer statistics, 2007," *Ca-Cancer J. Clin.* **57**, 43–66 (2007).
2. "1990 recommendations of the International Commission on Radiological Protection," in *ICRP Publication 60*, Pergamon, New York (1991).
3. V. Ntziachristos, J. Ripoll, L. V. Wang, and R. J. Weissleder, "Looking and listening to light: the evolution of whole-body photonic imaging," *Nat. Biotechnol.* **23**, 313–320 (2005).
4. R. Weissleder and V. Ntziachristos, "Shedding light onto live molecular targets," *Nat. Methods* **9**, 123–128 (2003).
5. T. H. Pham, F. Bevilacqua, T. Spott, J. S. Dam, B. J. Tromberg, and S. Anderson-Engels, "Quantifying the absorption and reduced scattering coefficients of tissue-like turbid media over a broad spectral range with non-contact Fourier-transform hyperspectral imaging," *Appl. Opt.* **39**, 6487–6497 (2000).
6. E. E. Graves, J. Ripoll, R. Weissleder and V. Ntziachristos, "A sub-millimeter resolution fluorescence molecular imaging system for small animal imaging," *Med. Phys.* **30**, 901–911 (2003).
7. D. Hall, G. Ma, F. Lesage, and Y. Wang, "Simple time-domain optical method for estimating the depth and concentration of a fluorescent inclusion in a turbid medium," *Opt. Lett.* **29**, 2258–2260 (2004).
8. S. H. Han and D. J. Hall, "Estimating the depth and lifetime of a fluorescent inclusion in a turbid medium using a simple time-domain optical method," *Opt. Lett.* **33**(9), 1035–1037 (2008).
9. S. Chandrasekhar, "Stochastic problems in physics and astronomy," *Rev. Mod. Phys.* **15**, 1–89 (1943).
10. M. S. Patterson, B. Chance, and B. C. Wilson, "Time resolved reflectance and transmittance for the noninvasive measurement of tissue optical properties," *Appl. Opt.* **28**, 2331–2336 (1989).
11. M. A. O'Leary, D. A. Boas, X. D. Li, B. Chance, and A. G. Yodh, "Fluorescence lifetime imaging in turbid media," *Opt. Lett.* **21**, 158–160 (1996).
12. V. Ntziachristos and R. Weissleder, "Experimental three-dimensional fluorescence reconstruction of diffuse media by use of a normalized Born approximation," *Opt. Lett.* **26**, 893–895 (2001).
13. D. Hall and S. H. Han, "Preliminary results from a Multi-wavelength time domain optical molecular imaging system," *Proc. SPIE* **6430**, 64300T (2007).
14. M. Firbank, M. Oda, and D. T. Depty, "An improved design for a stable and reproducible phantom material for use in near-infrared spectroscopy and imaging," *Phys. Med. Biol.* **40**, 955–961 (1995).
15. H. J. van Staveren, C. J. M. Moes, J. van Marle, S. A. Prahl, and M. J. C. van Gemert et al., "Light scattering in Intralipid-10% in the wavelength range of 400–1100 nm," *Appl. Opt.* **30**, 4507–4514 (1991).
16. K. Levenberg, "A method for the solution of certain non-linear problems in least squares," *Q. Appl. Math.* **2**(2), 164–168 (1944).
17. D. W. Marquardt, "An algorithm for least-squares estimation of non-linear parameters," *Soc. Indust. Appl. Math.* **11**(2), 431–441 (1963).